galaxies

MDPI

Article

Binary Interactions, High-Speed Outflows and Dusty Disks during the AGB-To-PN Transition

Raghvendra Sahai

Jet Propulsion Laboratory, California Institute of Technology, 4800 Oak Grove Drive, Pasadena, CA 91109, USA; sahai@jpl.nasa.gov; Tel.: +1-818-354-0452

Received: 9 July 2018; Accepted: 13 September 2018; Published: 25 September 2018

Abstract: It is widely believed that the dramatic transformation of the spherical outflows of AGB stars into the extreme aspherical geometries seen during the planetary nebula (PN) phase is linked to binarity and driven by the associated production of fast jets and central disks/torii. The key to understanding the engines that produce these jets and the jet-shaping mechanisms lies in the study of objects in transition between the AGB and PN phases. I discuss the results of our recent studies with high-angular-resolution (with ALMA and HST) and at high-energies (with GALEX, XMM-Newton and Chandra) of several such objects, which reveal new details of close binary interactions and high-speed outflows. These include two PPNe (the Boomerang Nebula and IRAS 16342-3814), and the late carbon star, V Hya. The Boomerang Nebula is notable for a massive, high-speed outflow that has cooled below the microwave background temperature, making it the coldest object in the Universe. IRAS 16342-3814 is the prime example of the class of water-fountain pre-planetary nebulae or PPNe (very young PPNe with high-velocity H_2O masers) and shows the signature of a precessing jet. V Hya ejects high-speed bullets every 8.5 years associated with the periastron passage of a companion in an eccentric orbit. I discuss our work on AGB stars with strongly-variable high-energy (FUV, X-ray) emission, suggesting that these objects are in the early stages of binary interactions that result in the formation of accretion disks and jets.

Keywords: planetary nebulae; AGB and post-AGB stars; binarity; accretion disks; jets; mass-loss; circumstellar matter; (sub)millimeter interferometry; ultraviolet radiation, X-rays

1. Introduction

The fundamental question that has motivated the Planetary Nebulae conference series is: How do the slowly expanding (5–15 km s^{-1}), largely spherical, circumstellar envelopes (CSEs) of AGB stars transform themselves into highly aspherical Planetary Nebulae (PNe), with collimated lobes and fast outflows ($\gtrsim few \times 100$ km s^{-1}) along one or more axes? The importance of collimated jets in forming ansae in PNe was recognized in [1]. Based on the wide variety of multipolar and point-symmetric morphologies seen in unbiased surveys of young PNe with HST, ref. [2] proposed that collimated fast winds or jets (hereafter, CFWs), operating during the pre-planetary nebula (PPN) or very late-AGB phase, are the primary agent for producing asymmetric shapes in PNe. The CFWs are likely to be episodic, and either change their directionality (i.e., axis wobbles or precesses) or have multiple components operating in different directions (quasi)simultaneously. These CFWs sculpt the AGB CSE from the inside-out, producing elongated bubbles or lobes within the CSEs. Later, additional action of the fast radiative wind from the central star may further modify these lobes, and ionization may lead to loss of some structure [3]. If a dense equatorial torus is present, it may add additional confinement for the CFWs, as well as for the spherical radiative wind from the hot central star at a later stage of evolution.

Binary star interactions are believed to underlie the formation of the overwhelming majority of PNe, which represent the bright end-stage of most stars in the Universe. Close binary interactions

also dominate a substantial fraction of stellar phenomenology, e.g., cataclysmic variables, type Ia supernovae progenitors, and low and high-mass X-ray binaries. Understanding the formation of aspherical PNe can help in addressing one of the biggest challenges for 21st century stellar astronomy—a comprehensive understanding of the impact of binary interactions on stellar evolution.

In this paper, I describe our observational techniques for searching for binarity (and signatures of associated active accretion) in AGB stars, as well as observational results from our recent studies of three key transition objects that have likely undergone recent (or are currently undergoing) close binary interactions. These objects show large and sudden mass-ejections prior to the formation of a planetary nebula, as well as disks, torii and (episodic) high-speed, collimated jets. Thus, they are Rosetta Stones for understanding aspherical PN formation. The paper is based on an invited talk that I gave at the Asymmetrical Planetary Nebulae (APN) VII meeting (Hong Kong, December 2017).

2. Binarity in AGB Stars

Observational evidence of binarity in AGB stars is difficult to come by because AGB stars are very luminous and variable, thus standard techniques for binary detection such as radial-velocity and photometric variations due to a companion star are not applicable. However, one can exploit the favorable secondary-to-primary photospheric flux contrast ratios reached in the UV for companions of spectral type hotter than about G0 (T_{eff} = 6000 K) and luminosity, L $\gtrsim$ 1 $L_{\odot}$. Ref. [4] (hereafter, Setal08) first used this technique, employing GALEX [5] to find emission from 9/21 objects in the FUV (1344–1786 Å) and NUV (1771–2831 Å) bands. Since these objects (hereafter, fuvAGB stars) also showed significant UV variability, setal08uv concluded that the UV source was unlikely to be solely a companion's photosphere, and was dominated by emission from variable accretion activity.

Accretion activity is likely to produce X-ray emission as well, as observed in young stellar objects [6]. A survey of archival XMM and ROSAT data found two AGB stars and the symbiotic star, Mira, with X-ray emission [7] . A pilot survey for X-ray emission from a fuvAGB stars using XMM-Newton and Chandra by [8] (hereafter, Setal15) detected X-ray emission in 3/6 fuvAGB stars observed. The X-ray fluxes were found to vary in a stochastic or quasi-periodic manner on roughly hour-long times-scales. These data, together with previous and more recent studies (Figure 1) and [9] , show that X-ray emission is found only in fuvAGB stars, with an FUV/NUV ratio $\gtrsim$ 0.17 (e.g., Table 1). There are two exceptions: V Hya and V Eri. The non-detection of V Hya, which has a high FUV/NUV ratio, is likely related to the fact that the companion is in an eccentric orbit, and the accretion rate, which is highly variable, was probably low when the X-ray observations were done (2.5 years after periastron passage) [10]; (hereafter Setal16). For V Eri, we can only speculate that the non-detection may be because V Eri was in a relatively low-accretion phase when the X-ray data were taken.

From modeling the X-ray spectra, Setal15 found that the observed X-ray luminosities are (0.002–0.11) $L_{\odot}$, and the X-ray emitting plasma temperatures are $\sim$(35–160)$\times 10^6$ K. These high X-ray temperatures argue against the emission arising directly in an accretion shock, unless it occurs on a white dwarf (WD) companion. However, none of the detected objects is a known WD-symbiotic star, suggesting that, if WD companions are present, they are relatively cool (<20,000 K). The high X-ray luminosities argue against emission originating in the coronae of MS companions. A likely origin of the X-ray emission is that it arises in hot plasma confined by magnetic fields associated with a disk around a binary companion. The plasma may be generated by an accretion shock on the disk that gives rise to the FUV emission in these objects. Based on the time-scale ($\sim$1.3 h) of the quasi-periodic variations in Y Gem—similar to the period of material orbiting close to the inner radius of an accretion disk around a sub-solar mass companion, i.e., with $M_c \lesssim 0.35\, M_{\odot}$ (implying a semi-major axis a $\lesssim 3 \times 10^{10}$ cm)—Setal15 argued that the most likely model for the X-ray emission from fuvAGB stars is that it arises at or near the magnetospheric radius in a truncated disk, or the boundary layer between the disk and star.

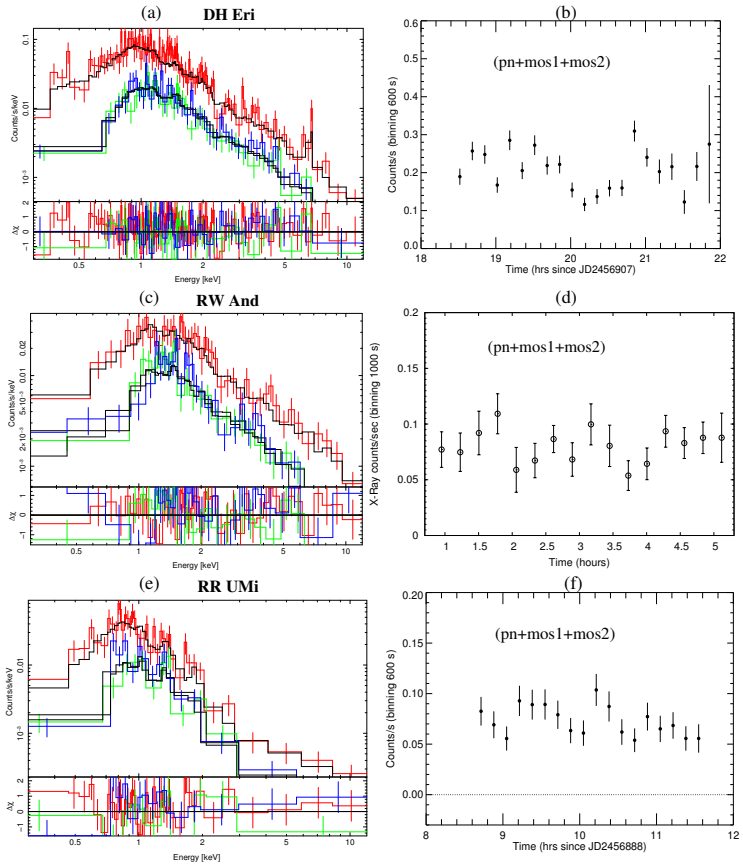

Figure 1. X-ray spectra (colored curves: XMM-Newton/EPIC pn, red; MOS1, green; and MOS2, blue) and model fits (black curves) of the fuvAGB stars DH Eri, RW And and RR UMi (panels **a**, **c**, **e**), and X-ray light curves (black symbols) (panels **b**, **d**, **f**). As for most fuvAGB stars, DH Eri and RW And are each fitted by a single hard component (Tx $\sim 5 \times 10^7$ K) (panels a & C, respectively), but in RR UMi (panel **e**) the dominant emission component has Tx that is significantly lower (Tx(1) $\sim 6.6 \times 10^6$ K); a weaker harder component (Tx(2) $\sim 10^8$ K) is also present (*adapted from Sahai, Sánchez Contreras and Sanz-Forcada 2018, in prep.*).

We note that, in RR UMi, which has a relatively low FUV/NUV ratio amongst the X-ray emitting fuvAGB stars, the X-ray spectrum has a hard and a soft component, with the softer one being more dominant (Figure 1e). We infer that, whereas the hard component is related to weak accretion activity, the soft one likely represents the expected coronal emission from the main-sequence (MS) companion. This hypothesis is supported by the fact that, in contrast to the other X-ray detected objects, RR UMi also has very low FUV variability (as expected when accretion activity is relatively weak).

We searched the Mikulski Archive for Space Telescopes (MAST) for GALEX data on fuvAGB stars, using a comprehensive input catalog of ∼4000 AGB stars (includes O-rich, C-rich and S-stars) collected from various published sources and searches for counterparts in the GALEX archive within a user-specified search radius. We have generated a photometric database that provides: (i) relevant parameters such as FUV and NUV fluxes, errors, and exposure times, for detected objects for each "visit", (ii) the background "sky-noise" for stars that were observed but not detected; and (iii) variability properties for each of the detected objects. We found about ∼100 fuvAGB stars in the FUV band at a $\gtrsim 5\,\sigma$ level. Even for the hottest sources in our catalog (spec. type M4), the detected FUV fluxes ($\gtrsim$20 μJy) are significantly in excess above photospheric emission. We found that many fuvAGB stars show strong UV variability as well (e.g., Y Gem: [11]), with time intervals where the FUV and NUV variations are correlated, suggesting changes in the emission measure and/or the obscuring column, and where they are anti-correlated, suggesting changes in the temperature of the emitting material.

We tabulate below, for AGB stars that have been observed at two or more epochs and have X-ray observations with adequate sensitivity (i.e., integration times greater than ∼5 ksec with XMM-Newton or Chandra), FUV variability measures (standard deviation/median or *var*1 and (maximum-minimum)/median or *var*2 and the FUV/NUV ratio, versus the presence/absence of X-ray emission. We found that the FUV variability measures also show a correlation (Table 1) with the absence/presence of X-ray emission, but somewhat weaker than that shown by the FUV/NUV ratio: excluding the special case of V Hya, 5/7 stars with X-ray emission have high FUV variability ($var1 > 0.23$, $var2 > 0.58$), whereas all four stars without X-ray emission have low FUV variability ($var1 < 0.19$, $var2 < 0.37$). We hypothesize that the variable X-ray and FUV emission is directly or indirectly related to variable accretion onto the accretion disk and/or the companion; however, our sample is small, and X-ray data on a larger number of objects with FUV variability is needed to test our hypothesis more robustly.

Table 1. UV Variability and X-Ray Emission of fuvAGB Stars.

Name	FUV *var*1 [1]	FUV *var*2 [1]	FUV/NUV	X-Ray?
Y Gem	1.9	5.13	1.3	Y
EY Hya	0.39	0.93	0.83	Y
CI Hyi	0.67	1.33	0.54	Y
RW And	0.23	0.58	2.3	Y
R UMa	0.15	0.36	1.0	Y
RR UMi	0.033	0.066	0.3	Y
UY Leo	0.30	0.73	0.24	Y?
V Hya [2]	0.27	0.54	1.7	N
V Eri	0.19	0.37	0.96	N
del01 Aps	0.012	0.024	0.11	N
NU Pav	0.13	0.26	0.11	N
EU Del	0.10	0.19	0.10	N

[1] $var1 = \sigma$/median, *var*2 = (max-min)/median. [2] eccentric orbit, X-ray data taken far from periastron passage.

A detailed UV spectroscopic study of Y Gem with HST/STIS by [12] (hereafter Setal18) reveals strong flickering in its UV continuum on time-scales of $\lesssim$20 s, a characteristic signature of an active accretion disk. The *TESS* mission, which can provide 1σ noise sensitivity in 2 min of 690 ppm for fuvAGB stars as faint as ∼8.9 mag in the *TESS* photometric band, can thus be used to detect optical flickering with amplitudes that are a factor ∼200 lower than that in the FUV. We expect that such data will reveal some combination of the ∼hour-long quasi-periodic variations as well as stochastic (flickering) variations, based on current UV and X-ray data for a few fuvAGB stars. In addition, new kinds of variability may become apparent, since 2-min cadence data of the very high photometric sensitivity that *TESS* can achieve has never been reported for AGB stars.

Ref. [13] compared the UV properties of their sample with those of 12 AGB stars with known binary companions [14] , and supported Setal08's inference that the detection of FUV emission in AGB stars is a strong indicator of binarity.

In contrast, ref. [15] claimed that GALEX-detected UV emission is an inherent characteristic of AGB stars (likely combination of photoshperic and chromospheric emission). Their conclusion is based on a sample of 468 AGB stars, in which they detected 179 in both bands and 38 in the FUV band. They stated that there is evidence that the NUV emission appears to vary in phase with visible light curves in a few AGB stars, and then concluded that the UV emission is an inherent characteristic of AGB stars, and not likely to be indicative of a binary. However, we note that an inspection of their Figure 1 (which shows the American Association of Variable Star Observers (AAVSO) visual light curves and the X-ray data for nine stars) reveals only one star (R Cet) for which the correlation between optical and X-ray variability is clearly seen. Furthermore, the GALEX FUV/NUV ratio for chromospheric emission is likely to be lower than 0.17, as, e.g., revealed by spectroscopic observations of chromospheric emission in two objects: ∼0.05–0.1 in TW Hor, ∼0.1 in the red supergiant α Ori.

Another mechanism for producing high-energy radiation from single AGB stars may be long-duration flares due to magnetic reconnection events, suggested to explain an X-ray flare from the only AGB star that has shown one—the primary of the symbiotic star, Mira [16]. A high-sensitivity search in two stars with inferred strong magnetic fields did not find X-ray emission [17]. Thus, the (admittedly scant) observations so far do not show a relationship between the presence of magnetic fields and high-energy emission from single AGB stars.

3. The Effects of Binarity

3.1. Large Episodic Mass-Ejections that End the AGB/RGB Phase

The well-studied carbon star, V Hya, shows evidence for high-speed, collimated outflows and dense equatorial structures (discussed below), and is a key object in understanding the early transition of AGB stars into aspherical PNe. Setal16 found that this star is ejecting massive high-speed compact clumps (hereafter, bullets) periodically, leading to a model in which the bullet ejection is associated with the periastron passage of a close binary companion in an eccentric orbit around V Hya with an orbital period of ∼8.5 years. The detailed physical properties of this ejection suggests that the companion approaches the primary very close to the latter's stellar envelope at every periastron passage, suggesting that V Hya is a good candidate where the binary interaction will result in a CE configuration (see also [18]).

IRAS 16342-3814 (hereafter, IRAS 16342) is the best studied and nearest (∼2 kpc) example of "water-fountain" PPN—a class of young PPNe with unusually fast radial H_2O outflows with $V_{exp} \gtrsim 50$ km s^{-1} [19] showing that jet activity is extremely recent ($\lesssim 100$ years, ref. [20]), and indicating that these objects have become PPNe fairly recently. Its morphology is well-resolved with optical (HST) and near-infrared (Keck Adaptive Optics) imaging [21,22]. Radio interferometry (VLA, VLBA) shows water masers spread over a range of radial velocities encompassing 270 km s^{-1} [23]. From a study in which emission from ^{12}CO J=3–2 and other molecular lines with $\sim 0\farcs35$ resolution was mapped using ALMA, ref. [24] (hereafter, Setal17) found that ∼455 years ago, the progenitor AGB star of IRAS 16342 underwent a sudden, very large increase (by a factor > 500) in its mass-loss rate; the average value over this period is $> 3.5 \times 10^{-4}\ M_\odot$ yr^{-1}The Boomerang Nebula, long understood as an "extreme" bipolar pre-planetary Nebula (PPN), is the coldest known object in the Universe, with a massive high-speed outflow that has cooled significantly below the cosmic background temperature [25]. ALMA observations confirmed this finding, and revealed unseen distant regions of this ultra-cold outflow (UCO), out to $\gtrsim$120,000 AU [26]. The very large mass-loss rate ($\sim 0.001\ M_\odot$ yr^{-1}) characterizing the UCO and the central star's very low-luminosity ($300 L_\odot$) are unprecedented, making it a key object for testing theoretical models for mass-loss during post-main sequence evolution and for producing the dazzling variety of bipolar and multipolar morphologies seen in PNe [27]. In the UCO, the mass-loss rate ($\dot{M}$) increases with radius, similar to its expansion velocity (V)—taking $V \propto r$, $\dot{M} \propto r^{0.9-2.2}$. The mass in the UCO is $\gtrsim 3.3\ M_\odot$, and the Boomerang's MS progenitor mass is $\gtrsim 4\ M_\odot$. The UCO's kinetic energy is very high, $KE_{UCO} > 4.8 \times 10^{47}$ erg, and the most likely source of this energy is the gravitational energy released via binary interaction in a common envelope event (CEE). The Boomerang's primary was an RGB or early-AGB star when it entered the CE phase; the companion finally merged into the primary's core, ejecting the primary's envelope that now forms the UCO.

Although numerical simulations of CEE are becoming increasingly sophisticated, they are still very uncertain and require strong observational constraints (e.g., [28] and references therein). The Boomerang is the youngest and least-evolved known example of such an interaction, and it already raises a potential difficulty for such simulations in that the UCO morphology does not appear to be concentrated towards the equatorial plane, as numerical simulations usually indicate. A detailed inspection of such simulations by Iaconi et al. [28] shows that the ejecta's mass distribution tends to become increasingly isotropic with time. Since the UCO is observed at an age that is a factor ~ 650 larger than the 2000-day timespan in these simulations, it is not implausible that the lower-density polar

regions seen on small scales in the simulation get filled in with time (e.g., small perturbations in the velocity vectors away from radial would allow material to move towards the axis). New simulations of CEE or grazing envelope ejection (GEE: ref. [29], and references therein) that can reproduce the relatively well-defined properties of the Boomerang Nebula, will be very useful in improving our understanding of this important channel for binary star evolution.

3.2. Central Disks and Torii

Like most bipolar or multipolar PPN, all three of the objects described above (Section 3.1) directly show the presence of compact, dense equatorial structures in the form of disks and/or torii. In V Hya, ref. [30] found, using HST STIS observations, a hot, central disk-like structure of diameter 0.″6 (240 AU at V Hya's distance of 400 pc) expanding at a speed of 10–15 km s^{-1}.

In IRAS 16342, the central region had (literally) remained in "shadow" because of its high optical depth at the longest wavelengths that it had been imaged (12 μm, ref. [31]). Setal17's ALMA study provided an unprecedented close view of this region, revealing a compact source in ^{29}SiO J=8-7 (v=0) emission and dust thermal emission at 0.89 mm. In addition, a high-density ($> 3.3 \times 10^6$ cm^{-3}) tilted torus is revealed in H^{13}CN J=4–3 emission. The torus has a size of 1300 AU, and its inclination is 43°, consistent with the axis of its bipolar lobes [21] and the high-velocity H_2O outflow axis [23]. The deprojected torus expansion velocity is $V_{tor} = 20$ km s^{-1}, and its expansion time-scale is 160 years.

In the Boomerang, Setal17 found a dense central waist of size (FWHM) ∼1740 AU×275 AU. The ^{12}CO J = 3–2 line profile from the central waist is relatively narrow and may include components due to rotation and expansion. Assuming its outer regions to be expanding, it has an age of $\lesssim$1925 years. The waist has a compact core seen in thermal dust emission at 0.87–3.3 mm, which harbors 4–7 $\times 10^{-4}$ $M_\odot$ of very large (∼mm-to-cm sized), cold (∼20–30 K) grains.

The sizes of the above equatorial structures are much larger than the observed/expected sizes of accretion or circumbinary disks. The formation process is not understood. Ref. [32] suggested that such waists can form via the interaction of a CFW with its progenitor AGB wind. The waist mass provides an important constraint on theoretical models—e.g., CE evolution would likely cause expulsion of most of the stellar envelope ([33] , leading to much larger values of the waist mass ($\sim 0.1 M_\odot$) than wind-accretion modes. Quantitative predictions of the expected size and mass of the waist would be very helpful in testing these theoretical models.

3.3. Collimated Jet-Like Outflows and Binary Accretion Modes

All of the objects discussed above show evidence for episodic, collimated jet-like outflows, but with significant differences. If the physical properties of the fast outflows in PPNe are accurately determined, these can be used to estimate the jet momentum, $M_j V_j$, and the accretion time-scale, t_{acc}, which in turn can constrain the class of binary interaction and associated accretion modes (e.g., Bondi–Hoyle–Lyttleton wind-accretion and wind Roche lobe overflow (wRLOF), via an innovative analytical modelling approach described by [34] (hereafter, BL14). In BL14's approach, the intrinsic jet momentum is estimated from the observed fast outflow's momentum, assuming that the interaction between the intrinsic jet outflow and the ambient circumstellar envelope is momentum-conserving.

In Y Gem, Setal18 found UV lines with P-Cygni-type profiles from species such as Si IV and C IV with emission and absorption features that are red- and blue-shifted by velocities of ∼500 km s^{-1} from the systemic velocity. Setal18 concluded, from these (and previous) observations, that material from the primary star is gravitationally captured by a low-mass MS companion, producing a hot accretion disk around the latter. The disk powers a fast outflow that produces blue-shifted features due to absorption of UV continuum emitted by the disk, whereas the red-shifted emission features arise in heated infalling material from the primary. The accretion luminosity implies a mass-accretion rate

$> 5 \times 10^{-7}\, M_\odot$ yr^{-1}. Setal18 concluded that Roche lobe overflow is the most likely binary accretion mode since Y Gem does not show the presence of a wind.

In V Hya, the collimated ejection of material is in the form of bullets, and the ejection axis flip-flops around an average orientation, in a regular manner. These data support a model in which the bullets are a result of collimated ejection from an accretion disk (produced by gravitational capture of material from the primary) that is warped and precessing, and/or that has a magnetic field that is misaligned with that of the companion or the primary star (Setal16). The average momentum rate of the bullet ejections is ($\sim 8.2 \times 10^{25}$ g cm s^{-2}), implying a minimum required accretion rate of $\dot{M}_a \sim 3.3 \times 10^{-8}\, M_\odot$ yr^{-1}. Since the secondary must get very close to the primary's stellar envelope at periastron passage (Setal16), the binary separation is comparable to the stellar radius (at 400 pc, $R_* \sim 2$ AU, see [35]), i.e., $a_{or} \sim 2$ AU, so the Roche-lobe overflow mode (RLOF) is the appropriate accretion mode, which can easily supply the required accretion rate.

IRAS 16342 shows two very high-speed, knotty, jet-like molecular outflows, whose axes are not colinear. The Extreme High Velocity Outflow (EHVO) and the High Velocity Outflow (HVO) have (deprojected) expansion speeds of 360–540 and 250 km s^{-1} and ages of 130–305 and $\lesssim$110 years. The spiral structure seen in the position-velocity (PV) plot of the HVO most likely indicates emission from a precessing high-velocity bipolar outflow, as inferred previously from near-IR imaging [22], that entrains material in the near and far bipolar lobe walls. The measured expansion ages of the above structural components imply that the torus (age$\sim$160 years) and the younger high-velocity outflow (age$\sim$110 years) were formed soon after the sharp increase in the AGB mass-loss rate. The relatively high momentum rate for the dominant jet-outflow in IRAS 16342 ($> 5 \times 10^{28}$ g cm s^{-2}) implies a correspondingly high minimum accretion rate of $\dot{M}_a = 1.9 \times 10^{-5}\, M_\odot$ yr^{-1}. Setal17 compared this rate with the expected mass-accretion rates derived for different accretion models shown in BL14's Figure 1, and concluded that standard Bondi–Hoyle–Lyttleton (BHL) wind-accretion and wind-RLOF models with WD or MS companions were unlikely; enhanced RLOF from the primary or accretion modes operating within common envelope evolution were needed. We revisit this conclusion because the BHL rate shown in BL14's Figure 1b is derived using the primary's AGB mass-loss properties $\dot{M}_w = 10^{-5}\, M_\odot$ yr^{-1} (and $V_w = 10$ km s^{-1}, together with assumed orbital separation $a_{or} = 10$ AU, companion mass $M_c = 0.6\, M_\odot$, primary mass $M_p = 1.0\, M_\odot$) and not the much higher value of $\dot{M} \sim 1.3 \times 10^{-4}\, M_\odot$ yr^{-1} (comparable to the mass-loss rate in IRAS16342), mentioned in BL14's Section 3.1 and referenced in the figure caption (E. Blackman, *priv. comm.*), so the expected BHL accretion rate could be quite high in IRAS16342. The BHL rate estimate is valid only if the orbital separation is much larger than the Roche-lobe radius, i.e., $a_{or} >> R_{roche}$. For IRAS 16342, we found that $R_{roche}/a_{or} = 0.38 + log(M_p/M_c) = 0.5 - 0.54$, assuming $M_c = 0.6 - 1\, M_\odot$ and $M_p \sim 4\, M_\odot$ (the primary was likely relatively massive, $\sim 4.5\, M_\odot$, in order to have experienced HBB, needed to produce the very enhanced ^{13}C/^{12}C ratio observed in this object). Since the progenitor AGB star of IRAS 16342 must have had a radius $\gtrsim$1 AU (e.g., Dijkstra et al. [36] modeled its SED using an M9III star with $T_{\rm eff}$ = 2670 K and R = 372 $R_\odot$), the binary separation must be $\gtrsim$5 AU in order for the BHL accretion rate to be valid. Hence, we considered $a_{or} > 5 - 10$ AU, and found $\dot{M}_{BHL} \lesssim (0.3 - 1) \times 10^{-5}\, M_\odot$ yr^{-1}, taking $\dot{M}_w = 3.5 \times 10^{-4}\, M_\odot$ yr^{-1} and $V_w = 23$ km s^{-1} for IRAS16342 from Setal17. We conclude that the HVO in IRAS 16342 is not driven by accretion via BHL, but requires wind-RLOF or modes that provide higher accretion rates.

The Boomerang's central region has an overall bipolar structure; in detail, this structure is comprised of multiple, highly collimated lobes on each side of the central disk, both in scattered light and in ^{13}CO J=3–2 emission. The velocity of the molecular material in the dense walls of the collimated lobes is not particularly high, and we expect it is likely to be substantially lower than the velocity of the unshocked jet-outflow that has carved out these lobes, since the jet outflow has interacted with a very massive envelope (the UCO). Optical spectroscopy, indicating that the pristine fast outflow may have a speed of about 100 km s^{-1} [37], support this expectation. Assuming momentum-conservation to derive the fast outflow momentum (as in BL14) is likely to provide a severe underestimate of

the intrinsic jet momentum—numerical simulations are needed. However, in this object, the UCO's extreme properties(see Section 3.1) directly imply CE evolution.

4. Concluding Remarks and Future Prospects

We discuss observational results that address several key aspects in our quest to understand binary interaction as the underlying cause for the formation of aspherical planetary nebulae from AGB stars. These include the use of UV and X-ray observations to establish the presence of binarity and associated active accretion in AGB stars, as well as high-angular resolution mm-wave and optical observations to study the properties of jet-like outflows in objects in transition from the AGB to the PN phase. Further progress now requires: (i) high-angular resolution mm-wave observations (e.g., with ALMA) of a large sample of PPNe (to derive the jet properties and the AGB mass-loss properties immediately preceding the transition to the post-AGB phase); (ii) studies of accretion activity in statistical samples of fuvAGB stars using UV spectroscopy and high-sensitivity, high-time-cadence photometry to detect flickering, e.g., with the *TESS* mission (to understand the prevalence of binarity and assoicated accretion activity in AGB stars as a class); and (iii) X-ray surveys of AGB stars, including those with known strong B-fields, e.g., to test the relationship of primary's B-field and X-ray emission, and those with low FUV/NUV flux ratios (to understand the contribution and properties of X-ray emission from the companion's corona).

Funding: This research was funded by Space Telescope Science Intsitute: GO 14713.001, and NASA: 12-ADAP12-0283, 17-ADAP17-0206.

Acknowledgments: I thank Eric Blackman for a helpful discussion related to binary acretion modes. The author's research described here was carried out at the Jet Propulsion Laboratory, California Institute of Technology, under a contract with NASA, and funded in part by NASA via an ADAP award, and an HST GO award (GO 14713.001) from the Space Telescope Science Institute.

Conflicts of Interest: The author declares no conflict of interest.

References

1. Soker, N. On the formation of ansae in planetary nebulae. *Astron. J.* **1990**, *99*, 1869–1882.
2. Sahai, R.; Trauger, J.T. Multipolar Bubbles and Jets in Low-Excitation Planetary Nebulae: Toward a New Understanding of the Formation and Shaping of Planetary Nebulae. *Astron. J.* **1998**, *116*, 1357–1366.
3. Sahai, R.; Morris, M.R.; Villar, G.G. Young Planetary Nebulae: Hubble Space Telescope Imaging and a New Morphological Classification System. *Astron. J.* **2011**, *141*, 134.
4. Sahai, R.; Findeisen, K.; Gil de Paz, A.; Sánchez Contreras, C. Binarity in Cool Asymptotic Giant Branch Stars: A GALEX Search for Ultraviolet Excesses. *Astron. J.* **2008**, *689*, 1274–1278.
5. Morrissey, P.; Conrow, T.; Barlow, T.A.; Small, T.; Seibert, M.; Wyder, T.K.; Budavári, T.; Arnouts, S.; Friedman, P.G.; Forster, K.; et al. The Calibration and Data Products of GALEX. *Astrophys. J. Suppl. Ser.* **2007**, *173*, 682–697.
6. Favata, F. Accretion, fluorescent X-ray emission and flaring magnetic structures in YSOs. *Mon. Not. R. Astron. Soc.* **2005**, *76*, 337.
7. Ramstedt, S.; Montez, R.; Kastner, J.; Vlemmings, W.H.T. Searching for X-ray emission from AGB stars. *Astron. Astrophys.* **2012**, *543*, A147.
8. Sahai, R.; Sanz-Forcada, J.; Sánchez Contreras, C.; Stute, M. A Pilot Deep Survey for X-Ray Emission from fuvAGB Stars. *Astrophys. J.* **2015**, *810*, 77.
9. Sahai, R.; Sanz-Forcada, J.; Sánchez Contreras, C. Variable X-Ray and UV emission from AGB stars: Accretion activity associated with binarity. *J. Phys. Conf. Ser.* **2016**, *728*, 042003.
10. Sahai, R.; Scibelli, S.; Morris, M.R. High-speed Bullet Ejections during the AGB-to-Planetary Nebula Transition: HST Observations of the Carbon Star, V Hydrae. *Astrophys. J.* **2016**, *827*, 92.
11. Sahai, R.; Neill, J.D.; Gil de Paz, A.; Sánchez Contreras, C. Strong Variable Ultraviolet Emission from Y Gem: Accretion Activity in an Asymptotic Giant Branch Star with a Binary Companion? *Astrophys. J.* **2011**, *740*, L39.

12. Sahai, R.; Sánchez Contreras, C.; Mangan, A.S.; Sanz-Forcada, J.; Muthumariappan, C.; Claussen, M.J. Binarity and Accretion in AGB Stars: HST/STIS Observations of UV Flickering in Y Gem. *Astrophys. J.* **2018**, *860*, 105.
13. Ortiz, R.; Guerrero, M.A. Ultraviolet emission from main-sequence companions of AGB stars. *Mon. Not. R. Astron. Soc.* **2016**, *461*, 3036–3046.
14. Famaey, B.; Pourbaix, D.; Frankowski, A.; van Eck, S.; Mayor, M.; Udry, S.; Jorissen, A. Spectroscopic binaries among Hipparcos M giants,. I. Data, orbits, and intrinsic variations. *Astron. Astrophys.* **2009**, *498*, 627–640.
15. Montez, R., Jr.; Ramstedt, S.; Kastner, J.H.; Vlemmings, W.; Sanchez, E. A Catalog of GALEX Ultraviolet Emission from Asymptotic Giant Branch Stars. *Astrophys. J.* **2017**, *841*, 33.
16. Soker, N.; Kastner, J.H. Magnetic Flares on Asymptotic Giant Branch Stars. *Astrophys. J.* **2003**, *592*, 498–503.
17. Kastner, J.H.; Soker, N. Constraining the X-Ray Luminosities of Asymptotic Giant Branch Stars: TX Camelopardalis and T Cassiopeia. *Astrophys. J.* **2004**, *608*, 978–982.
18. Barnbaum, C.; Morris, M.; Kahane, C. Evidence for Rapid Rotation of the Carbon Star V Hydrae. *Astrophys. J.* **1995**, *450*, 862.
19. Likkel, L.; Morris, M.; Maddalena, R.J. Evolved stars with high velocity H2O maser features—Bipolar outflows with velocity symmetry. *Astron. Astrophys.* **1992**, *256*, 581–594.
20. Imai, H. Stellar molecular jets traced by maser emission. In *Astrophysical Masers and Their Environments*; Chapman, J.M., Baan, W.A., Eds.; IAU Symposium: Paris, France, 2007; Volume 242, pp. 279–286.
21. Sahai, R.; te Lintel Hekkert, P.; Morris, M.; Zijlstra, A.; Likkel, L. The "Water-Fountain Nebula" IRAS 16342-3814: Hubble Space Telescope/Very Large Array Study of a Bipolar Protoplanetary Nebula. *Astrophys. J. Lett.* **1999**, *514*, L115–L119.
22. Sahai, R.; Le Mignant, D.; Sánchez Contreras, C.; Campbell, R.D.; Chaffee, F.H. Sculpting a Pre-planetary Nebula with a Precessing Jet: IRAS 16342-3814. *Astrophys. J. Lett.* **2005**, *622*, L53–L56.
23. Claussen, M.J.; Sahai, R.; Morris, M.R. The Motion of Water Masers in the Pre-Planetary Nebula IRAS 16342-3814. *Astrophys. J.* **2009**, *691*, 219–227.
24. Sahai, R.; Vlemmings, W.H.T.; Gledhill, T.; Sánchez Contreras, C.; Lagadec, E.; Nyman, L.Å.; Quintana-Lacaci, G. ALMA Observations of the Water Fountain Pre-planetary Nebula IRAS 16342-3814: High-velocity Bipolar Jets and an Expanding Torus. *Astrophys. J. Lett.* **2017**, *835*, L13, doi:10.3847/2041-8213/835/1/L13.
25. Sahai, R.; Nyman, L.Å. The Boomerang Nebula: The Coldest Region of the Universe? *Astrophys. J. Lett.* **1997**, *487*, L155–L159.
26. Sahai, R.; Vlemmings, W.H.T.; Huggins, P.J.; Nyman, L.Å.; Gonidakis, I. ALMA Observations of the Coldest Place in the Universe: The Boomerang Nebula. *Astrophys. J.* **2013**, *777*, 92.
27. Balick, B.; Frank, A. Shapes and Shaping of Planetary Nebulae. *Ann. Rev. Astron. Astrophys.* **2002**, *40*, 439–486.
28. Iaconi, R.; Reichardt, T.; Staff, J.; De Marco, O.; Passy, J.C.; Price, D.; Wurster, J.; Herwig, F. The effect of a wider initial separation on common envelope binary interaction simulations. *Mon. Not. R. Astron. Soc.* **2017**, *464*, 4028–4044.
29. Shiber, S.; Soker, N. Simulating a binary system that experiences the grazing envelope evolution. *Mon. Not. R. Astron. Soc.* **2018**, *477*, 2584–2598.
30. Sahai, R.; Morris, M.; Knapp, G.R.; Young, K.; Barnbaum, C. A collimated, high-speed outflow from the dying star V Hydrae. *Nature* **2003**, *426*, 261–264.
31. Verhoelst, T.; Waters, L.B.F.M.; Verhoeff, A.; Dijkstra, C.; van Winckel, H.; Pel, J.W.; Peletier, R.F. A dam around the Water Fountain Nebula?. The dust shell of IRAS16342-3814 spatially resolved with VISIR/VLT. *Astron. Astrophys.* **2009**, *503*, 837–841.
32. Soker, N.; Rappaport, S. The Formation of Very Narrow Waist Bipolar Planetary Nebulae. *Astrophys. J.* **2000**, *538*, 241–259.
33. Nordhaus, J.; Blackman, E.G. Low-mass binary-induced outflows from asymptotic giant branch stars. *Mon. Not. R. Astron. Soc.* **2006**, *370*, 2004–2012.
34. Blackman, E.G.; Lucchini, S. Using kinematic properties of pre-planetary nebulae to constrain engine paradigms. *Mon. Not. R. Astron. Soc.* **2014**, *440*, L16–L20.
35. Knapp, G.R.; Jorissen, A.; Young, K. A 200km/s molecular wind in the peculiar carbon star V Hya. *Astron. Astrophys.* **1997**, *326*, 318–328.

36. Dijkstra, C.; Waters, L.B.F.M.; Kemper, F.; Min, M.; Matsuura, M.; Zijlstra, A.; de Koter, A.; Dominik, C. The mineralogy, geometry and mass-loss history of IRAS 16342-3814. *Astron. Astrophys.* **2003**, *399*, 1037–1046.
37. Neckel, T.; Staude, H.J.; Sarcander, M.; Birkle, K. Herbig-Haro emission in two bipolar reflection nebulae. *Astron. Astrophys.* **1987**, *175*, 231–237.

© 2018 by the authors. Licensee MDPI, Basel, Switzerland. This article is an open access article distributed under the terms and conditions of the Creative Commons Attribution (CC BY) license (http://creativecommons.org/licenses/by/4.0/).